This article was published as: Phil. Trans. R. Soc. A 377: 20180218.

DOI : http://dx.doi.org/10.1098/rsta.2018.0218

PHILOSOPHICAL TRANSACTIONS A

Phil. Trans. R. Soc. A.
doi:10.1098/not yet assigned

Mechanical properties of magnetic gels containing rod-like composite particles

Mariem M. Abrougui[1], Modesto T. Lopez-Lopez[2,#], Juan D. G. Duran[2,*]

[1] Centre National des Recherches en Sciences des Materiaux, Technopole Borej Cedria, BP 73, 8027 Soliman, Tunisia; and Faculté des Sciences de Tunis, Université de Tunis El Manar, Tunisie B.P. 94-Rommana, 1068, Tunisia

*[2] Department of Applied Physics, Faculty of Sciences, University of Granada, 18071, Granada, Spain, #ORCID ID 0000-0002-9068-7795; *ORCID ID 0000-0002-5586-1276*

Keywords: Hydrogel, ferrogel, magnetorheology, sepiolite, magnetite, alginate

Summary

Magnetic gels (ferrogels) are heterogeneous systems structured at the nanoscale that contains magnetic particles dispersed in 3-D networks of polymer chains. In the present work, the magnetic particles were synthesized with a core-shell structure, consisting of sepiolite particles covered by magnetite nanoparticles. These composite particles had a rod-like shape with a high aspect ratio. The obtained sepiolite-magnetite particles showed a high enough susceptibility and saturation magnetization. The magnetorheological (MR) properties, and the intensity of the MR effect, of aqueous suspensions of the synthesized particles, were studied. The particles, functionalized by adsorption of alginate molecules, were imbedded in alginate hydrogels to get homogeneous soft materials. The particles were linked to the polymer chains as the knots in a network and dominated in a great extent the mechanical properties of the materials. After determining the optimal compositions of the ferrogels, their viscoelastic properties were measured in the absence/presence of magnetic fields. The results pointed out that the MR effect provided by the clay-magnetite particles was considerably more intense than those achieved in ferrogels that contain spherical magnetic microparticles. Therefore, the imbedding of rod-shaped magnetic particles in hydrogels allows controlling the mechanical properties in a wider range than in conventional ferrogels.

1. Introduction

Magnetic hydrogels (or ferrogels) are magnetisable soft and wet materials non-existing in nature. They are heterogeneous materials that belong to a more general group of soft materials usually called magnetic colloids. These materials are mainly characterized by their smart nature because the action of external magnetic fields can control the macroscopic properties of these systems. They can be classified, depending on the continuous phase in which the magnetic particles are dispersed, in two groups: i) magnetic suspensions (1), and ii) magneto-polymers (2). In the first ones, the continuous phase is a Newtonian liquid (aqueous solution or oil). There are two kinds of suspensions: ferrofluids (FF) and magnetorheological suspensions (MRS), which essentially differ in the particle size of the particles. In FF the particles are less than about 50 nm (magnetically monodomain) while in MRS they are in the micrometric scale (multidomain). In the second group (magneto-polymers), the magnetic particles can be dispersed in and highly elastic (and dry) polymer network, that is an elastomer, as for example synthetic rubber. In magnetic elastomers the mechanical properties (Young and shear moduli) can be strongly modulated by applying external magnetic fields (3, 4). Alternatively, the continuous phase can be a soft viscoelastic gel consisting of polymer chains extended across oil or aqueous solution (2, 5). The present work is devoted to these soft-wet materials, called magnetic hydrogels or ferrogels.

Magnetic hydrogels are one the most versatile magnetic colloids because their macroscopic properties

*Author for correspondence (jdgarcia@ugr.es).
†Present address: Department of Applied Physics,
Faculty of Sciences, University of Granada, 18071, Granada, Spain

(particularly the mechanical ones) can be modified in very different ways due to the complexity of their internal structure at the nano- and micrometric scale. These systems can be designed modifying different parameters as follows. i) The composition, concentration, size and shape of the magnetic particles. ii) The length, chemical composition, and the concentration of the polymer chains. iii) The crosslinking degree of the polymer network. iv) The density of bonds (if they exist) among the polymer chains and the magnetic particles. v) Finally, the degree of hydration (swelling by water), which can reach more than 90 % v/v (6, 7).

In addition, magnetic hydrogels can be provided of the required biocompatibility for their use in biomedical applications such as controlled drug delivery or reparation/regeneration of damaged biological tissues (5, 8, 9). In tissue engineering, magnetic hydrogels can work as scaffolds to generate artificial tissues. For this purpose, the magnetic particles have to be functionalized, and the polymer usually is a natural polymer, to avoid the immune response (10).

In the majority of the ferrogels reported in the literature, the particles have a spherical shape, being composed of ferromagnetic metals (iron) or ferrites (magnetite). In these cases, a problem arises because the high density of the particles can favour their gravitational settling during the ferrogel preparation and, in consequence, the resulting gel has a poor homogeneity. This problem can be overcome using core-shell composites (magnetite-polymer, iron-silica) (6, 7, 10, 11), although usually spherical-shaped particles are employed because of the simplicity of the synthesis procedure.

In the present work, the magnetic particles consisted of sepiolite microparticles covered by magnetite nanoparticles. Sepiolite is a clay mineral with a rod-like (or fibre) shape with a high aspect ratio (length/thickness ratio). In addition, the high porosity of this mineral favours that their fine pores act as seeds for the growth of magnetite nanoparticles and, as a consequence, the formation of a composite with a high enough magnetic response. Their low average density hinders the settling during the crosslinking of the pre-gel mixture, which is a sodium alginate solution. Even more, the sepiolite-magnetite particles were functionalized by adsorption of alginate molecules prior to their mixture with the pre-gel solution. This functionalization favour the formation of bonds among the particles and the alginate chains during the gelation process and the resulting ferrogel is a polymer network reinforced by particle knots.

Besides the preparation of the sepiolite-magnetite-alginate hydrogels, in the present work a rheological characterization of the clay-magnetite aqueous suspensions and of the corresponding ferrogels is carried out, both in the absence and in the presence of external magnetic fields. The objective is to quantify the intensity of the magnetorheological effect achieved in these heterogeneous systems.

2. Materials and experimental methods

2.1. Materials

The sepiolite particles, supplied by Sigma-Aldrich (USA), with a specific surface area 300 m^2/g (12), were homoionized substituting the exchangeable cations by Na ions as follows: 25 g of sepiolite powder were dispersed in 250 mL of 1 M NaCl solution and stirred during 1 h. After that, the particles were separated by centrifugation and then redispersed in a 1 M NaCl solution. This process was repeated five times. Finally, the particles were repeatedly redispersed/centrifuged in deionized water (Milli-Q Academic, Millipore, France) until the conductivity of the supernatant was below 20 μS/cm. Finally, the particles were dried at 90 ºC and stored. The homoionized sepiolite particles will be called SP particles in what follows.

The chemicals employed in the synthesis of sepiolite-magnetite particles were $FeCl_3 \cdot 6H_2O$, NH_4OH aqueous solution (25 % NH_3), and $FeCl_2 \cdot 4H_2O$ (98 %). For the preparation of the hydrogels, the chemicals employed were $CaCl_2$ (99 %), $CaCO_3$ (99 %), D-glucono-δ-lactone (GDL), and sodium alginate [empirical formula $(C_6H_7NaO_6)n$]. All these chemicals were supplied by Sigma-Aldrich (USA), and used without any further purification.

2.2. Synthesis and functionalization of the magnetite-covered sepiolite particles

The synthesis route of the sepiolite-magnetite particles (SM particles in what follows) used in the present work was adapted from a previous one reported by Liu et al. (13) for the preparation of attapulgite-magnetite composites. The synthesis involves the following steps:

i) First, 1.5 g of SP particles were dispersed in a solution of 4.4104 g $FeCl_3 \cdot 6H_2O$ in 200 mL of deionized water.
ii) The suspension was kept during 30 min in an ultrasonic bath. Then, it was deoxygenated by bubbling nitrogen during 15 min. Finally, the flask was closed and the suspension magnetically stirred during 12 h.
iii) Then, 1.6136 g of $FeCl_2 \cdot 4H_2O$ were added to the suspension obtained in step (ii). This new suspension was heated at 90 ºC and, after that, 6 mL of NH_4OH was rapidly added under stirring. A black precipitate appeared immediately. The resulting suspension was stirred in nitrogen atmosphere during 1 h at 90 ºC.
iv) The mixture obtained in step (iii) was cooled down to room temperature and, finally, washed by repeated cycles of decantation (using a powerful magnet) and redispersion in fresh water until the supernatant conductivity was less than 20 μS/cm.

In parallel, pure magnetite nanoparticles were synthetized following the same procedure just described but, obviously, without adding (step i) sepiolite particles in the reaction medium.

The magnetite-covered sepiolite particles were functionalized by adsorption of sodium alginate (SMA particles in what follows). For this purpose, 1.0 g of SM particles were dispersed in a solution that contained 0.25 g of sodium alginate in 50 mL of water. This suspension was mechanically stirred at room temperature during 1 h. Then, the suspension was cleaned as described in point (iv) above.

2.3. Preparation of the magnetic hydrogels

The magnetic hydrogels, consisting of SMA particles dispersed in an alginate hydrogel, were prepared by a similar procedure to that described in ref. (7), as it follows:

i) A suspension with a concentration of 10 % w/v of SMA particles was prepared by mechanical stirring in deionized water.
ii) Two different solutions of sodium alginate were prepared. The first, containing 0.25 g of alginate in 50 mL of water (0.5 % w/v), and the second one with 0.5 g of alginate in 50 mL of water (1 % w/v).
iii) Aliquots of 2.5 mL of the suspension prepared in step (i) were mixed with 2.5 mL of each one of the two different alginate solutions prepared in step (ii). These two pre-gel mixtures were carefully shaken by hand until the resulting suspensions were homogeneous.
iv) Then, 22.5 mg of $CaCO_3$ were added to each one of the pre-gel suspensions prepared in the previous step and stirred by a vortex mixer during a few seconds.
v) An amount of 26.7 mg of GDL was added to the mixture, shaking it then by hand, and placing it afterwards in a Petri dish at rest during 4 h.
vi) Finally, 5 mL of a 45 mM $CaCl_2$ solution was added and the mixture wasleft overnight at room temperature until obtaining the final ferrogel.

Note that the Ca ions are the crosslinkers that promote the formation (gelation) of the alginate hydrogel. The GDL molecules (added in step v) hydrolyse in water solution to gluconid acid, so imparting the required acidification for the decomposition of calcium carbonate. In this way, the slow liberation of calcium ions in the aqueous medium allows obtaining homogeneous ferrogels. The calcium solution added in step (vi) provokes the swelling, as well as the final crosslinking (by diffusion of Ca^{2+}), in order to get gels with high enough consistence. The two ferrogels obtained, using the 0.5 % w/v or, alternatively, the 1 % w/v alginate solution, will be called in what follows “Ferrogel-1” and “Ferrogel-2”, respectively.

2.4. Characterization of the particles and gels

The chemical composition of the sepiolite particles (before homoionization) was determined by X-ray fluorescence (Philips Magix Pro PW-2440 apparatus), in which the major elements present in the sample were determined in the form of oxides.

The zeta potential of the particles was determined from electrophoretic mobility (EM) measurements in a Malvern Zeta-Sizer Nano SZ (Malvern Instruments, UK) at 25 ºC. For these measurements, different dilute suspensions (less than 1 % w/v) of SP, magnetite, SM and SMA particles were prepared in a solution with constant ionic strength (1 mM NaCl) and the pH adjusted in the interval between pH 4 and pH 10. Then, the suspensions were kept during 24 h and the pH readjusted immediately before the EM measurements. Each value of the zeta-potential reported is the average of at least 9 measurements.

The size and shape of the SP particles and the SM and SMA composites were observed by high resolution scanning electron microscopy (SEM) using a Zeiss SUPRA40VP (USA) microscope. The microstructure of the

ferrogels was observed in a Quanta 650 Field-Emission Environmental Scanning Electron Microscope (FEI, USA). In this case, and for avoiding the modification of the original structure of the hydrogel, the sample was previously prepared by the so-called Critical Point Drying (CPD) technique. This technique essentially consists of the substitution of the water in the hydrogel by carbon dioxide and later removing the CO_2 by increasing temperature and pressure up to the critical point.

The magnetic properties of the composite particles (SM, SMA) were measured at room temperature in a vibrating sample magnetometer VSM 4500 (EG&G Princeton Applied Research, USA). First, the samples (dry powders) were magnetized varying the external field intensity (H) from 0 to 374 kA/m to obtain the first magnetization curve and, second, the magnetization loop was obtained varying H along the cycle 374 – 0 – (-374) – 0 – 374 kA/m. For each H value the corresponding magnetization (M) was obtained.

2.5. Rheological measurements

The rheological properties of the SM and SMA suspensions were measured at 25 ± 0.1 ºC in a Haake MARS III rheometer using titanium double cone-plate geometry with 600 mm diameter and 2º-cone apex (DC 60/2º Ti L, Thermo Fisher Scientific USA). The magnetic field was applied in the vertical direction (perpendicular to the rheometer plate) by an external coil. The magnetic field intensity in the sample position reaches up to 43 kA/m.

The rheological characterization of the ferrogels was carried out at 25 ± 0.1 ºC in a magneto-rheometer Physica MCR 300 (Thermo Fisher Scientific, USA) using plate-plate geometry with 20 mm in diameter. The plates have a rough surface to avoid wall slipping. The magnetic field applied, in the range 0 – 282 kA/m, was perpendicular to the plates that confined the samples. The ferrogels samples were carefully taken out from the Petri dish and placed in the bottom plate of the rheometer. A normal force as low as 0.1 N was kept on the disk-like samples to ensure a good contact between the rotor plate and the samples, and the gap between the plates was slightly varied according to that condition. The samples were in contact with a vapour-saturated atmosphere for avoiding their drying during the rheological measurements. In addition, a fresh sample was used for each measure to ensure reproducibility of the initial conditions.

In the case of the SM and SMA suspensions, two different measurements protocols were performed: i) steady-state measurements, and ii) dynamic measurements (oscillometry). In the first one, a shear stress ramp was applied and the corresponding shear rate was measured, obtaining the rheograms that characterize the samples, both in the absence and in the presence of magnetic field. The time between two consecutive steps in the shear ramp was 5 s.

In oscillometry, the same protocol was employed for both the SM or SMA suspensions and for the ferrogels. The objective was to obtain the values of the viscoelastic moduli (G' elastic or storage modulus, G" loss or viscous modulus) that characterize the viscoelastic response of the material to a shear stress. The samples were subjected to a sinusoidal shear strain, maintaining a constant frequency (1 Hz) and increasing the strain amplitude (γ_0) from very low to high enough values up to reaching a non-linear viscoelastic response. In the non-linear region, G' and G" strongly depend on γ_0. On the contrary, the region of low strain, in which G' and G" are practically independent of γ_0, corresponds to the viscoelastic linear region. These tests were also performed in the absence and in the presence of magnetic fields of increasing intensity. The delay time between two consecutive steps in γ_0 was 5 s for the suspensions and 10 s for the ferrogels.

3. Results and discussion

3.1. Particle characterization

The bulk chemical composition of the sepiolite particles (prior to the homionization) is included in Table S1 (supplementary material). The sepiolite clay is a hydrated magnesium aluminium silicate in which Mg and Fe substitute Al in a high extent in the octahedral layers (14). Nevertheless, in the sepiolite employed in this work, the Mg ions are largely dominants, being Al and Fe in a much smaller concentration.

For checking the coverage of the sepiolite particles by magnetite nanoparticles and then by alginate molecules, the zeta potential of the particles was determined in suspensions with variable pH and constant ionic strength (1 mM NaCl). Figure 1 shows the results obtained. In the case of magnetite, the zeta potential is positive below the isoelectric point (iep) at pH ≈ 5.5, and negative for larger pH values (up to pH = 10), as a consequence of

the adsorption of H^+ and OH^- ions that usually are potential determining ions for metal oxides. The value of the pH(iep) of magnetite nanoparticles in the literature is usually around the value obtained in the present work (15, 16), although values as high as pH(iep) = 8 have also been reported (17).

The zeta potential of the homoionized sepiolite particles (SP, Figure 1) is negative in the entire pH interval studied. This is usual in other similar compounds as silica, bentonite, and homoionized montmorillonite (15, 18, 19). Nevertheless, in sepiolite clays it seems that the interfacial potential is strongly dependent on the origin and treatment of the clay particles. For natural sepiolite (without any physical or chemical treatment) the particles have an isoelectric point at pH ≈ 6 (20, 21), although the substitution of the exchange divalent cations by monovalent ones provokes that the positive branch of the zeta-potential, at pH < pH(iep), disappears (21). In fact, when natural palygorskite clays, which have a structure and chemical composition practically identical to sepiolite (14), are treated with solutions of alkaline ions or, alternatively, dispersed in acid solution to remove impurities as carbonates, the zeta potential reported have negative values at acid and also at basic pH (13, 22, 23). Therefore, when the impurities are removed or the exchange multivalent cations are replaced by monovalent ones, the electrochemistry of the solid/liquid interface of the sepiolite particles is mainly dominated by the reactions with the silanol (Si-O-H) groups, as for silica particles occurs.

The negative surface charge of the SP particles favours the adsorption of the Fe(III) and Fe (II) ions, and the subsequent formation of magnetite particles when OH^- ions are added. In this reaction, the pores in the SP particles act as seeds for the growth of magnetite nanoparticles. The zeta potential of the resulting particles (SM, Figure 1) is clearly the result of such coverage. A similar behaviour was reported for magnetite-covered attapulgite (13) (attapulgite and palygorskite are synonymous). In a recent work (24), devoted to the synthesis of magnetite-covered sepiolite, the pH corresponding to the point of zero charge of the composite particles was found at pH = 6.6, in between of those corresponding to sepiolite (pH = 7.4) and magnetite (pH = 4.8).

Finally, the SM particles were functionalized by adsorption of alginate molecules and, as a consequence, the zeta potential suffers a significant increase in absolute value (SMA, Figure 1). In principle, the adsorption of alginate molecules, negatively charged because of the dissociation of the carboxylic group, on the negatively charged particles, should be hindered by electrostatic repulsion. Nevertheless, the great affinity of carboxylate ions for the Fe and Si ions presents in the surface of these composite particles provokes their chemisorption by formation of coordinate compounds. This behaviour has been extensively observed in similar systems in which polyelectrolytes that bear carboxylate groups forms surface compounds with clay minerals or iron oxides (17, 25, 26).

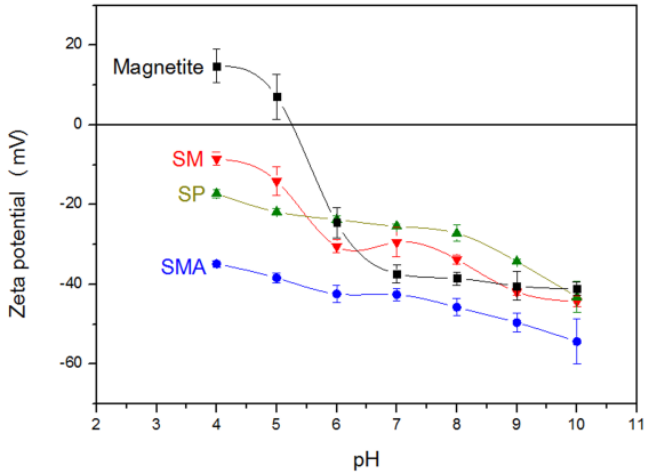

Figure 1. Zeta potential as a function of the pH in suspensions of the indicated particles. SP: homoionized sodium sepiolite paricles. SM: magnetite-covered SP particles. SMA: SM particles with alginate molecules adsorbed. Ionic strength of the solution 1 mM NaCl.

The morphology of the SP, the composite particles, and the ferrogels were observed by electron microscopy (see Figure 2). The SP particles (Figure 2a) show their typical rod-like or fibre shape with a high aspect ratio: the particle length/diameter is around 1 μm/0.1 μm, although both length dimensions present a great polydispersion. In the composite particles (SM, Figure 2b), spheroidal granules of magnetite nanoparticles appear attached on the surface of the SP particles. In fact, the EDX (electron dispersive X-ray) microanalysis carried out in the same SEM microscope clearly demonstrated the presence of significant amounts of iron

atoms: the peaks of Fe had practically the same intensity than the Si ones. The pictures of the SMA particles (Figure 2c) show that the alginate layer favours a more smooth surface texture than that in the SM particles.

More interestingly, for the goal of the present work, Figure 2d shows the microstructure of the magnetic hydrogel (Ferrogel-1). In this picture the more brilliant regions (coloured in false light blue) correspond to the heavier atoms (silicon and manly iron), while the less brilliant (brown colour) corresponds to the lighter atoms. Thus, we can clearly distinguish the magnetic composites (SMA) from the polymer fibres. The particles seem not only randomly embedded in the polymer network, but also linked by multiple bonds to the alginate chains. This fact, let us point something that demonstrates the relevant role played by the alginate molecules adsorbed on the particles: both the alginate molecules in the pre-gel solution and those previously adsorbed on the particles should be cross-linked to each other by calcium ions. Therefore, the SMA particles are imbedded as knots in a highly entangled network, what will have important effects on the magneto-rheological response of the ferrogels, as we will see in section 3.3.

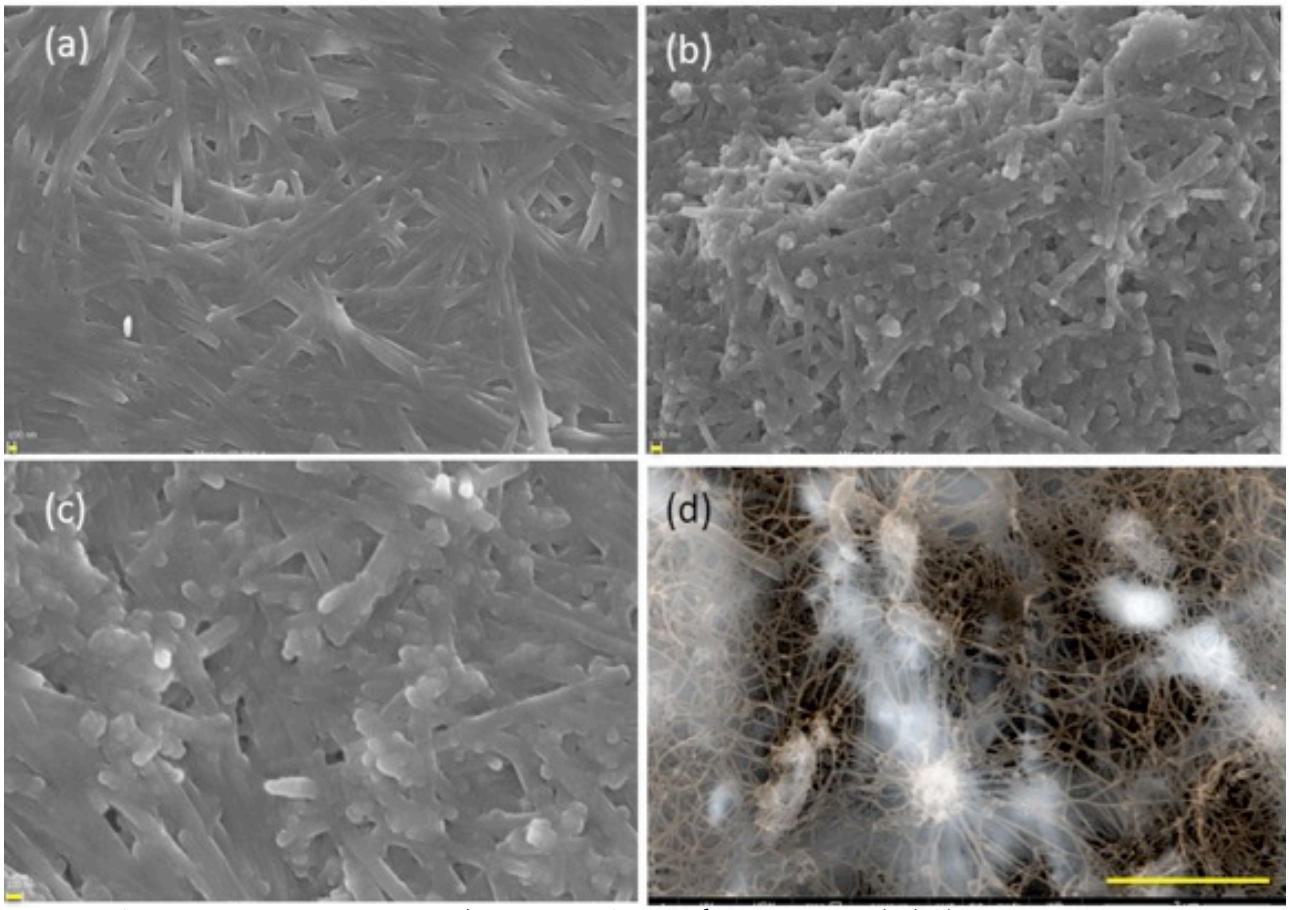

Figure 2. Electron microscopy pictures of: a) SEM – sepiolite after homoionization (SP); b) SEM - magnetite-covered sepiolite (SM); c) SEM - SM particles covered by alginate (SMA); d) environmental SEM - ferrogel (SMA particles in alginate hydrogel). Bar lengths in yellow: (a), (b), (c) 100 nm (see short line at lower left corner); d) 3 μm.

As mentioned in the Introduction section, one of the advantages of using the SM composite particles is their low average density, as compared with that of pure magnetite, which would hinder their gravitational settling in the pre-gel solution. Unfortunately, the SM particles settled too fast in water as shown in Figure S1 (supplementary material). Note that in the total balance of the colloidal forces in clay or clay composite suspensions, usually the long-range van der Waals attraction dominates on the (shorter range) electrostatic repulsion (15). Likely, the resultant colloidal force among the particles gives raise to bundle-like aggregates that settled in less than an hour, which was too fast considering the slow kinetics of the gelation process. On the contrary, the SMA suspension remained stable (Figure S1) enough time for avoiding the phase separation during the gelation time. We have to take into account that the molecular weight of the sodium alginate employed ranges between 80,000 - 120,000 g/mol. Thus, the alginate layer provoked a strong electro-steric repulsion among the SMA particles that consequently remained as individual entities or as aggregates of only a few particles (see Figure 2d).

The following step in the particle characterization was to analyse the magnetic properties of the obtained composite particles. Figure 3a shows the first magnetization curve of the SM and SMA dry powders, that is the magnetization (M) as a function of the applied magnetic field intensity (H) in the range from 0 kA/m to 374 kA/m. The magnetic susceptibility (χ) and saturation magnetization (M_S) of the SM and SMA particles can be estimated by fitting the data to the Frölich-Kennely equation (27):

$$M = \frac{\chi M_S H}{M_S + \chi H} \quad [1]$$

The best fitting parameters were: For SM powder: χ = 4.61 ± 0.08, M_S = 216.3 ± 1.0 kA/m (coefficient of determination r^2 = 0.992); and for SMA: χ = 6.55 ± 0.13, M_s = 169.9 ± 0.6 kA/m (r^2 = 0.988). In addition, the real content of magnetic phase in the composite particles can be obtained by considering the mixing law (28):

$$M_{S,C} = \phi M_{S,m} \quad [2]$$

where $M_{S,C}$ and $M_{S,m}$ are the saturation magnetization of the composite particles (SM or SMA) and bulk magnetite, respectively, and ϕ the volume fraction of magnetite in the solid particles. Taking into account that $M_{S,m}$ = 446 kA/m (29), the content of magnetic material in the SM and SMA particles was ϕ(SM) = 48 % and ϕ(SMA) = 38 %. These results seem reasonable because the presence of the alginate layer in SMA particles diminishes the relative volume concentration of magnetite in the composite.

In Figure 3b the magnetization loops are included. Both powders behaved as magnetically soft materials because the remnant magnetization (M_R) and the coercitivity (H_C) were almost negligible. Their values (see the plot inserted in Figure 3b) were: M_R = 1.0 kA/m, H_C = -0.18 kA/m for SM powder; and M_R = 0.3 kA/m, H_C = -0.04 kA/m for SMA powder. This soft behaviour in the SM composites has also been stated in a recent work that describes a different synthesis route for obtaining magnetite-covered sepiolite particles (24).

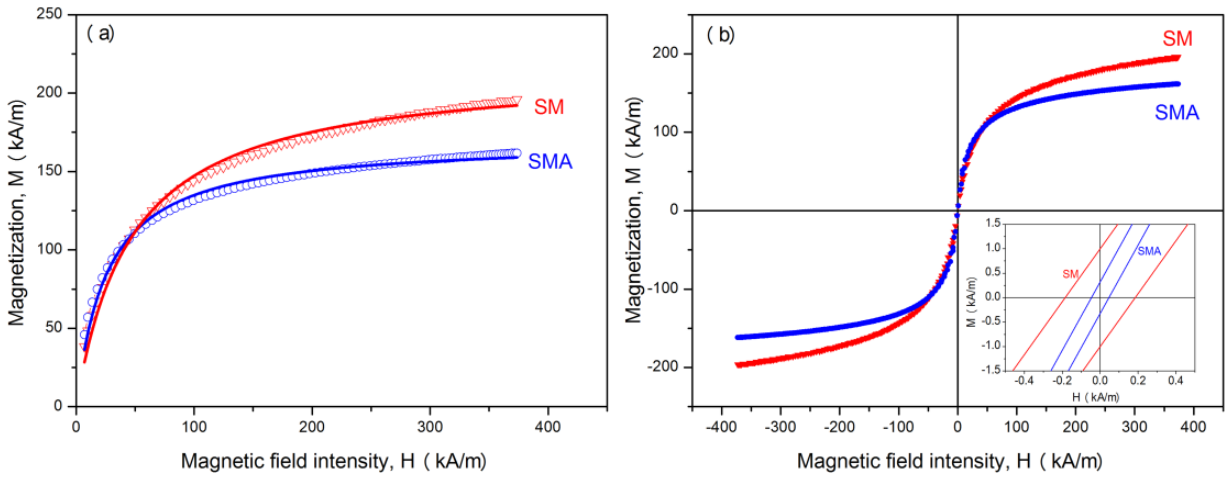

Figure 3. Magnetization as a function of the intensity of the applied magnetic field for SM and SMA composite powders. a) First magnetization curve; the lines correspond to the best fits to equation [1]. b) Magnetization loop, H varies along the cycle 374 – 0 – (-374) – 0 – 374 kA/m; the insert shows the region of very low field.

3.2. Rheology of the suspensions

Before analysing the magneto-rheological behaviour of the magnetic hydrogels, it is convenient to study the MR response of the SM and SMA suspensions for determining the particle concentration required for: i) Achieving a high enough MR effect, and ii) obtaining homogeneous ferrogels. This second point must be considered because an excessive particle concentration provokes the formation of lumpy or too fragile (or even fissured) ferrogels, as demonstrated in a previous work with iron/alginate ferrogels (7).

The rheograms (shear stress vs. shear rate) of SM and SMA suspensions are included in Figure S2 (supplementary material). The particle concentration range does not exceed 10 % w/v because of the above-mentioned requirement (ii). In both suspensions, the application of even a stress as low as 1 Pa leads to shear

rates $\dot{\gamma} \approx 100\ s^{-1}$. In the SM suspensions (Figure S2a) and, especially for the higher concentrations (7% and 10 % w/v), there are two regions in the rheograms. For low rates they behave as shear-thinning: the slope of the rheogram (the viscosity) decreases progressively; while for high rates they behave as a shear-thickening (the viscosity increases). For example, for 7% and 10 % concentrations, the transition occurs at $\dot{\gamma} = 90\ s^{-1}$. This transition from shear-thinning to shear-thickening has been described by Wagner and Brady (30) considering the balance between hydrodynamic and Brownian forces given by the Péclet number:

$$\mathrm{Pe} = \frac{\sigma a^3}{kT} \qquad [3]$$

where σ is the shear stress, a the hydrodynamic radius, k the Boltzmann constant, and T the temperature. Following the description given in ref. (30), there are three regions: i) for Pe < 1, the viscosity is constant (Newtonian fluid), ii) for Pe = 1 – 10 the viscosity decreases (shear-thinning behaviour), and iii) for Pe > 10 the viscosity increases (shear-thickening). In the 7% and 10 % w/v SM suspensions, for $\dot{\gamma} \approx 90\ s^{-1}$ the shear stress $\sigma \approx 0.5$ Pa, and taking $a \approx 1$ μm, the Peclet number is Pe = 122, well into the region of hydrodynamic-driven interactions. From a microscopic point of view, in this region the hydrodynamic forces provoke the formation of hydroclusters in which the particles are impeded to flow around each other, which leads to an abrupt increase in viscosity. The analysis in ref. (30) was done for concentrated ($\phi > 10$ %) suspensions of spherical particles. Although we have suspensions with not so high particle concentration, the particles are far from being spherical and, consequently, the formation of clusters with difficult internal movement at high shear can appear at much smaller particle concentration than for spheres. Even more, if we consider that, as demonstrated in previous works (31, 32), in fibre-like suspensions the particle-particle solid friction considerably hinders the relative movement of particles inside bundle-like aggregates. In addition, as predicted in ref. (30), when the particles are functionalized with large molecules, imparting electro-steric repulsion between the particles, the viscosity values reached in the shear-thickening region are considerably reduced. In fact, this decrease is evident if we compare the maximum viscosities reached in the 7 % and 10 % SM suspensions (9.5 mPa·s and 10.7 mPa·s, respectively) with those in SMA suspensions (6.9 mPa·s and 9.6 mPa·s).

The next question arises about the strength of the MR effect in SM and SMA suspensions with 10 % w/v concentration. For this purpose, the corresponding rheograms (see Figure S3, supplementary material) were obtained in the range of low-moderate magnetic fields. For SM suspensions (Figure S3a), the general trends of the rheograms obtained with magnetic field applied are similar to those in the absence of field: a first shear-thinning region (up to $\dot{\gamma} \approx 70\ s^{-1}$) followed by a shear thickening region, although the most important feature is the high MR effect. If we quantify the intensity of the MR effect (at a given shear rate) as

$$\text{MRE-}\sigma\ (\%) = \frac{\sigma(H \neq 0) - \sigma(H = 0)}{\sigma(H = 0)} \times 100 \qquad [4]$$

Then, for example, at $\dot{\gamma} = 100\ s^{-1}$ and H = 43 kA/m, MRE (%) = 7650 % which is large enough taking into account that the particle concentration is 10 % w/v, and that the content of magnetite in the solid phase is 48 % v/v.

In the SMA suspensions the trends of the rheograms under field application (Figure S3b) are completely different of those in SM suspensions. The shear-thickening region observed at H = 0 has disappears and, in the curves for H > 0, only a slight shear-thinning behaviour remains. More interestingly, the MR effect is considerably weak in comparison with the SM suspension: At $\dot{\gamma} = 100\ s^{-1}$ and H = 43 kA/m, MRE (%) = 360 %. This decrease in the MR effect can be explained considering that the functionalized SMA particles bear a layer of alginate molecules that impose a steric barrier to the field-induced chaining of the particles. If the particles are not in close contact, the dipole-dipole magnetic interaction is significantly smaller and, consequently, the MR effect is reduced.

The results in Figure S3b correspond to the steady-state magnetorheology of the suspensions when they suffer a very large shear strain. However, when the particles are imbedded into the polymer network they will be slightly strained before the breakage of the hydrogel. Therefore, it seems convenient to determine the MR behaviour of the SMA suspensions in conditions of small strain. This study can easily be performed by oscillometry for obtaining the elastic modulus in the absence and presence of magnetic field. The results obtained for SMA suspensions are represented in Figure 4. In these plots there is a first region in which the

elastic modulus (G') weakly depends on the strain amplitude (γ_0) (the viscoelastic linear region, VLR) followed by an abrupt decrease in G' when the field-induced structures of the systems are disrupted (the non-linear viscoelastic region, N-VLR).

In the VLR, the elastic modulus (G') slowly increases with the strain up to a maximum (the critical strain, γ_c) before going into the N-VLR. The critical strain can be interpreted as the strain reached immediately before the breakage of the microstructures of the suspensions. As demonstrated in previous works (31, 32), in suspensions of fibre-like magnetic particles, the progressive increase in G' in the VLR is due to the rising in the (field-dependent) static friction between the particles inside the bundle-type columns generated by the field. The values of G' at γ_c can be taken to quantify the intensity of the MR effect, by means of:

$$\text{MRE-G' (\%)} = \frac{G'(H \neq 0) - G'(H = 0)}{G'(H = 0)} \times 100 \qquad [5]$$

Taking G'(H = 43 kA/m) and G'(H = 0) from Figure 4, the intensity of MR effect given by equation [5] for SMA suspensions is 5814 %. This value is higher than that obtained in a previous work (33) with suspensions of ferromagnetic Co-Ni nanofibres (56 nm length; 5 % v/v concentration) in which MRE-G' (%), in the field range 0 – 57 kA/m, was around 500 %, although certainly the Co-Ni particles were smaller than the SMA particles. A better comparison could be done with another previous work (34) with suspensions of iron fibres (5.4 - 7.6 microns in length; 2 - 6 % v/v concentration), in which the MR effect was determined by estimating the dynamic (or Bingham) yield stress of the suspensions under field application. In that work, for a magnetic flux density of around 50 mT, the maximum yield stress reached (longest particles, highest concentration) was around 1.2 kPa, while in the absence of field the yield stress was approximately 0.1 kPa. Taking these values, the intensity of the MR effect (equation [4]) would be around 1100 %, which is an intermediate value between those calculated by equation [4] for the SM suspension (7650 %) and SMA (360 %) suspensions (see above). Note that this comparison (equation [4]) corresponds to experimental conditions in which the field-induced structure of the suspensions is completely broken, while the comparison by means of equation [5] (previous paragraph) is related to the strain at the initial breakage of the suspensions.

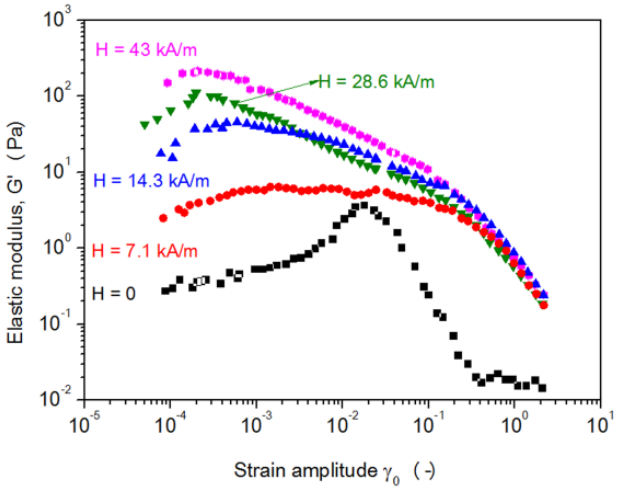

Figure 4. Elastic modulus as function of the strain amplitude (at constant frequency of 1 Hz) for SMA suspensions at 10 % w/v in the presence of the indicated magnetic fields.

3.3. Rheology of magnetic hydrogels

For the preparation of the magnetic hydrogels, 2.5 mL of the 10 % w/v suspension of SMA particles were mixed with 2.5 mL of alginate solutions and 5 mL of $CaCl_2$ solution, and also with 22.5 mg of $CaCO_3$ and 26.7 mg of GDL (section 2.3). Then, the final concentration of SMA particles in the ferrogels was 2.5 % w/v. Thus, the expected MR effect of the ferrogels will be lower than this of the SMA suspensions due to the smaller concentration of the magnetic particles and also because the particles will be dispersed in a viscoelastic solid (the hydrogel) instead of water. In addition, the moderate fields (up to H = 43 kA/m) achieved by the coil available in the rheometer Mars III (employed for SM and SMA suspensions) were not able to provoke a significant strengthening of the ferrogels. For this reason, the characterization of the ferrogels was carried out

in a magneto-rheometer Physica MCR 300 in which the field applied to the samples is considerably more intense.

Two different ferrogels were prepared with different alginate concentrations in the pre-gel solution (step (ii) in section 2.3): 0.25 g/50 mL (0.5 % w/v) in "Ferrogel-1", and 0.5 g/50 mL (1 % w/v) in "Ferrogel-2". Figure 5 shows the viscoelastic moduli obtained as the amplitude of the shear strain was increased in a wide enough interval to sweep from the VLR to well into the N-VLR. The moduli were measured for H = 0 and for strong magnetic fields (H > 100 kA/m).

Firstly, it is interesting to comment the behaviour in the absence of magnetic field. The two ferrogels prepared behave as viscoelastic solids because G' > G" in the VLR, which extends up to the critical strain $\gamma_c \approx 3$ (300 %), where a maximum in G" was reached. At the critical strain (300 %), the microstructure of the hydrogels began to break and the hydrogels behave as viscoelastic liquids (G" > G') with a progressive lower stiffness (both G' and G" suffered a quick drop).

Secondly, the different alginate concentrations in both studied ferrogels provoked that the Ferrogel-2 (F2) was significantly more rigid in the VLR than the Ferrogel-1 (F1). Thus, the G' values were (Table 1) as follows. i) For a strain amplitude $\gamma_0 = 0.03$ (3 %), G' (F1) = 20550 Pa and G' (F2) = 27180 Pa, which represents a relative increment of 32.3 % in the elastic response. ii) For $\gamma_0 = 0.1$ (10 %), G' (F1) = 28450 Pa and G' (F2) = 35810 Pa, increment 25.8 %. These last values are close to those reached at maximum in the G'-γ_0 curves which are: G' (F1) = 30590 Pa and G' (F2) = 38660 Pa, increment 26.3 %.

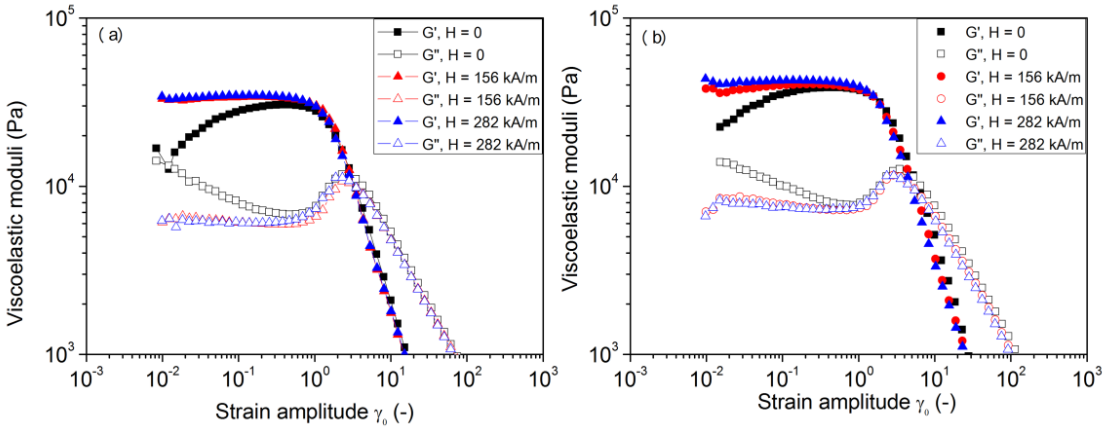

Figure 5. Viscoelastic moduli (G' solid symbols; G" open symbols) as a function of the strain amplitude for the indicated magnetic field intensities. Frequency 1 Hz. a) "Ferrogel-1"; b) "Ferrogel-2"(see section 2.3).

In addition, in the two ferrogels, in the absence of field, as the strain increases up to $\gamma_c \approx 300$ % the elastic response is progressively larger. This behaviour is not usual in elastic solids because, in the VLR, G' is practically constant. Nevertheless, we have to take in mind that the microstructure of these gels is a network in which the knots are occupied by magnetic particles linked to the polymer chains. In consequence, at very low strain a part of the net will be relaxed (lower G') and then, as the network is progressively stretched more and more branches withstand the mechanical stress. This fact, at the macroscopic scale, implies a progressive increase in G'. Obviously, when the maximum stretching is exceeded the break point is reached.

On the other hand, when an external field was applied, the magnetic particles located in the knots of the net were brought closer and the elastic modulus should increase, leading to a significant MR effect in the ferrogels. This effect is evident for low enough strain values, approximately for $\gamma_0 < 1$ (100 %). Nevertheless, as the network was stretched the magnetic particles were compelled to separate and the dipole-dipole magnetic force decayed, and the MR effect was progressively lower. Finally, as the critical strain was approached (as occurred in the absence of field), the mechanical response of the gels depended only on the network deformation. For this reason, all the curves independently of the field applied collapsed at a relatively large strain (300 %).

The data in Tables 1 and 2 indicated that the intensity of the MR effect depended on the strain amplitude, the magnetic field intensity, and the alginate concentration in the pre-gel solution, as summarized below.

i) Strain amplitude. The highest values of the MR effect (MRE-G', equation [5]) were reached for the lowest values of strain amplitude. Thus, when γ_0 increases from 3 % (Table 1) to 10 % (Table 2) the MRE-G' values were approximately reduced to the third part in the Ferrogel-1 (from 60-64 % to 19-22 %) and also in the Ferrogel-2 (from 38-53 % to 12-19 %), being practically null for $\gamma_0 > 1$ (100%).

ii) Magnetic field. When the applied field approached 300 kA/m, the maximum MR effect achieved was 64 % in Ferrogel 1 ($\gamma_0 = 3$ %) and the minimum was 19 % for Ferrogel-2 (at $\gamma_0 = 10$ %). The increase of the MRE-G' values, as H went from 156 to 282 kA/m, was relatively low in practically all cases (only for Ferrogel-2 at $\gamma_0 = 3$ % there was a moderate increment from 38 to 53 %), indicating that for large enough fields (H > 100 kA/m) the MRE was close to saturation. This is logical if one takes into account that the saturation magnetization of the SMA particles was $M_S = 169.9$ kA/m and the slope of the first magnetization curve was considerably reduced for fields larger than approximately 100 kA/m.

iii) Alginate concentration. This was the dominant factor facing the magnetic-induced reinforcement of the magnetic gels because an excessively rigid hydrogel (as in Ferrogel-2) hindered at a large extent the MR effect achieved. And, on the contrary, if the hydrogel contained a very low volume density of cross-linked chains the resulting ferrogels were too soft to be handled.

Table 1. Intensity of the MR effect for "Ferrogel-1" and "Ferrogel-2" (see section 2.3) obtained from data in Figure 5. MRE-G' % calculated by means of equation [5]. $\Delta G' = G'(H \neq 0) - G'(H = 0)$.

Strain amplitude $\gamma_0 = 0.03$ (3%)				
Sample (alginate concentration in pre-gel solution)	H (KA/m)	G' (Pa)	ΔG' (Pa)	MRE-G' (%)
"Ferrogel-1" (0.5 g/50 mL)	0	20550	–	–
	156	32980	12430	60
	282	33610	13060	64
"Ferrogel-2" (1 g/50 mL)	0	27180	–	–
	156	37480	10300	38
	282	41700	14520	53

Table 2. Similar to Table 1, but for a strain amplitude $\gamma_0 = 0.1$.

Strain amplitude $\gamma_0 = 0.1$ (10 %)				
Sample (alginate concentration in pre-gel solution)	H (KA/m)	G' (Pa)	ΔG' (Pa)	MRE-G' (%)
"Ferrogel-1" (0.5 g/50 mL)	0	28450	–	–
	156	33960	5510	19
	282	34600	6150	22
"Ferrogel-2" (1 g/50 mL)	0	35810	–	–
	156	40050	4240	12
	282	42500	6690	19

The intensity of the MR effect reached in the present work, especially with Ferrogel-1 (up to 64 %) is not negligible in comparison with those reached in previous works, even employing magnetic particles with a high saturation magnetization or larger particle concentrations. For example, in ref. (11), using polymer-covered magnetite spheres (diameter 110 nm) in a fibrin-agarose hydrogel the MR effect was 8 %. In other recent work (7), with silica-covered iron spheres (diameter 1.4 μm) in alginate hydrogel, the MRE-G' value was around 700 %. Nevertheless, a more quantitative comparison can be made if we consider, as Bossis et al. stated in ref. (1), that the shear modulus in suspensions of magnetic microparticles is proportional to the applied field (H), the particle saturation magnetization (M_S), and the particle volume fraction (Φ). Thus, we can define a normalized MRE-G' parameter, taking into account the different magnetic response of the particles (through the M_S), the maximum field applied in each case, and the particle concentration in the ferrogels by means of the following dimensionless expression:

$$\overline{MRE}(\%) = (MRE - G')(\%)\frac{M_{S,0}}{M_S}\frac{H_{max,0}}{H_{max}}\frac{\Phi_0}{\Phi} \qquad [6]$$

where MRE-G′ is the MR effect calculated by equation [5]. H_{max}, M_S and Φ are, respectively, the maximum field applied to the ferrogel, the magnetization saturation of the particles, and the particle volume fraction (% v/v) in the ferrogels studied in refs. (7, 11). The quantities with subscript "0" correspond to the Ferrogel-1: $H_{max,0}$ = 282 kA/m, $M_{S,0}$ = 169.9 kA/m, and Φ_0 = 0.93 % v/v (the particle concentration in Ferrogel-1 is 2.5 %w/v, and the average density of the SMA particles is 2.7 g/cm^3). In this manner, the $\overline{MRE}(\%)$ values mainly depend on the shape of the particles imbedded in the ferrogels. From these data, and the corresponding $\overline{MRE}(\%)$ values summarized in Table 3, we can deduce that:

i) The rod-like particles in the Ferrogel-1 provoked a considerably larger (normalized) MR effect (64 %) than the spherical magnetite particles in the magnetite/fibrin-agarose ferrogel in ref. (11) (11.4 %). Even more, taking into account that the fibrin-agarose hydrogels (without particles) are softer (rigidity modulus G = 47 Pa; ref. (11)) than the alginate ones (without particles, G′ ≈ 10^3 Pa; ref. (7)).

iii) The composite particles employed in the present work provided a more intense magnetic control of the mechanical properties that that achieved using iron microspheres in alginate ferrogels (7), in which the (normalized) MR effect is 15.2 %. The difference is even more pronounced if we remember that the volume fraction of the magnetisable material in the clay-magnetite composites was ϕ(SMA) = 38 % while, in the silica-covered particles in ref. (7), the iron volume fraction is ϕ(Fe) = 93 %. This last value has been calculated taken M_S(bulk Fe) = 1710 kA/m (27), M_S (iron powder) = 1587 kA/m (7), and the mixing law given by equation [2].

In summary, the rod-shaped SMA composite particles allow to obtain a higher efficiency in enhancing the MR response in ferrogels than those containing spherical magnetisable particles.

Table 3. Comparison among the MR effects achieved in different magnetic hydrogels (see text).

Ferrogel (reference)	Composition (Particles /Polymer in hydrogel)	M_S (kA/m)	H_{max} (kA/m)	Φ (% v/v)	MRE-G′ (%)	$\overline{MRE}(\%)$
Ferrogel-1 (present work)	Rod-like Fe_3O_4-sepiolite /Alginate	169,9 (*)	282 (*)	0.93 (*)	64	64
Ref. (11)	Spherical polymer-Fe_3O_4 / Fibrin-agarose	161	48.6	3.5 (**)	8 (**)	11.4
Ref. (7)	Spherical silica-Fe /alginate	1587	282	4.6 (***)	700 (**)	15.2

(*) $M_{S,0}$, $H_{max,0}$, and Φ_0 in equation [6]
(**) Taken from Fig. 5 in ref. (11)
(***) Taken from Fig. 10 in ref. (7)

4. Conclusions

Ferrogels are soft-wet materials with an internal nanostructure that, under magnetic field application elongate along the magnetic field lines and, when the field disappears, recover their previous isotropic structuration. Such local field-induced structuration, as very recently Borin et al. (35) stated, confers to the ferrogels their metastable (far from thermodynamic equilibrium) and transitive non-ergodic character. This character can be achieved if the ferrogels accomplish two conditions: First, they should be homogeneous at the macroscopic scale and, second, they should possess a strong enough response to external magnetic fields. These requirements demand a careful design of the system architecture at the nanoscale, from the magnetic particle composition up to the polymer network and, preferably, also in the linkage between the particles and the polymer chains.

Bearing in mind these arguments, in the present work, the ferrogels consisted of composite microparticles, with a core of low density (sepiolite clay) covered by a layer of magnetite nanoparticles, dispersed in a

polymer network composed by alginate molecules crosslinked by calcium ions. The crosslinking is due to electrostatic attractions among the Ca ions and the alginate molecules, instead of by covalent bonds because this last usually generates too rigid hydrogels, in which the orientation of the particles along the field lines is avoided. In addition, the magnetic particles were functionalized for enabling the formation of links among the particles and the polymer chains in the hydrogel. Thus, the resulting ferrogels presented an internal structure with the particles imbedded in the hydrogel as the knots in a network.

The magnetite layer on the clay particles was thick enough for conferring to the composite particles a high enough magnetic response, capable of providing a very high MR effect in aqueous suspensions, even for 10 % w/v particle concentration.

The SMA/alginate ferrogels, containing a particle volume fraction as low as 0.93 % v/v, presented a MR effect up to 64 %, under application of magnetic fields with intensity around that required for the magnetic saturation of the particles. The MR effect reached significant values for shear strains lower than 10 %. At higher strains, the viscoelastic response of the magnetic gels was predominantly determined by the resilience of the polymer-particle network, and the magnetic forces lost their influence because of the large gap between the particles.

The rod-like shape of the composite particles plays a central role in conditioning the intensity of the MR effect. In fact, we used a parameter for the quantification of the MR effect that only takes into account the particle shape (normalizing by the saturation magnetization, the applied field, and the particle volume fraction). Using this parameter, such effect in ferrogels with rod-like particles (64 %) becomes considerably larger than those reached in ferrogels with spherical microparticles (11 - 15 %).

Acknowledgments. This study was supported by project FIS2017-85954-R (Ministerio de Economía, Industria y Competitividad, MINECO, and Agencia Estatal de Investigación, AEI, Spain, cofunded by Fondo Europeo de Desarrollo Regional, FEDER, European Union). The authors are also grateful to Dr. Pavel Kuzhir (Institut de Physique de Nice, Université Côte d'Azur, CNRS; Nice, France) for his help in measuring the magnetic properties of the powders.

5. References

1. Bossis G, Volkova O, Lacis S, Menier. In: Odenbach S, editor. Magnetorheology: Fluids, structures and rheology. Springer, Bremen; 2002. Chapter 11, pp. 202–230. (doi: 10.1007/3-540-45646-5)
2. Lopez-Lopez MT, Durán JDG, Iskakova LY, Zubarev AY. 2016. Mechanics of Magnetopolymer Composites: A Review. *J Nanofluids* **5**, 479–495. (doi: https://doi.org/10.1166/jon.2016.1233)
3. Varga Z, Filipcsei G, Zrínyi M. 2006. Magnetic field sensitive functional elastomers with tuneable elastic modulus. *Polymer* **47**, 227-233. (https://doi.org/10.1016/j.polymer.2005.10.139)
4. Agirre-Olabide I, Berasategui J, Elejabarrieta MJ, Bou-Ali MM. 2014. Characterization of the linear viscoelastic region of magnetorheological elastomers. *J Intell Mater Syst Struct* **25**, 2074–2081. (doi: 10.1177/1045389X13517310)
5. Datta P. Magnetic gels. In: Kunal PK, Banerjee I, editors. Polymeric Gels Characterization, Properties and Biomedical Applications. Woodhead Publishing, Elsevier; 2018. Chapter 17 pp. 441- 465. (https://doi.org/10.1016/B978-0-08-102179-8.18001-9)
6. Bonhome-Espinosa AB, Campos F, Rodriguez IA, Carriel V, Marins JA, Zubarev A, Duran JDG, Lopez-Lopez MT. 2017. Effect of particle concentration on the microstructural and macromechanical properties of biocompatible magnetic hydrogels. *Soft Matter* **13**, 2928-2941. (doi: 10.1039/c7sm00388a)
7. Gila-Vilchez C, Bonhome-Espinosa AB, Kuzhir P, Zubarev A, Duran JDG, Lopez-Lopez MT. 2018. Rheology of magnetic alginate hydrogels. *J. Rheol.* **62**, 1083–1096. (https://doi.org/10.1122/1.5028137)
8. Culver HR, Clegg JR, Peppas NA. 2017. Analyte-responsive hydrogels: Intelligent materials for biosensing and drug delivery. *Acc. Chem. Res.* **50**, 170–178. (doi: 10.1021/acs.accounts.6b00533)
9. Li Y, Huang G, Zhang X, Li B, ChenY, LuT. 2013. Magnetic hydrogels and their potential biomedical applications. *Adv. Funct. Mater.* **23**, 660–672. (https://doi.org/10.1002/adfm.201201708)
10. Lopez-Lopez MT, Scionti G, Oliveira AC, Duran JDG, Campos A, Alaminos M, Rodriguez IA. 2015. Generation and characterization of novel magnetic field-responsive biomaterials. *PLOS ONE 10*, e0133878. (doi:10.1371/journal.pone.0133878)
11. Zubarev A, Bonhome-Espinosa AB, Alaminos, Duran JDG, Lopez-Lopez MT. 2018. Rheological properties of magnetic biogels. *Arch Appl Mech* Published online: 24 August 2018. (https://doi.org/10.1007/s00419-018-1450-2)

12. Valentinia F, Diamantia, Carbonea M, Bauerb EM, Palleschia G. 2012. New cleaning strategies based on carbon nanomaterials applied to the deteriorated marble surfaces: A comparative study with enzyme based treatments. *App Surf Sci* **258**, 5965–5980. (doi:10.1016/j.apsusc.2012.01.076)
13. Liu Y, Liu P, Su Z, Li F, Wen F. 2008. Attapulgite–Fe3O4 magnetic nanoparticles via co-precipitation technique. *App Surf Sci* **255**, 2020-2025. (doi: 10.1016/j.apsusc.2008.06.193)
14. Murray HH. Traditional and new applications for kaolin, smectite, and palygorskite: a general overview. 2000. *App Clay Sci* **17**, 207–221. (doi: 10.1016/S0169-1317(00)00016-8)
15. Galindo-Gonzalez C, Vicente J, Ramos-Tejada MM, Lopez-Lopez MT, Gonzalez-Caballero F, Duran JDG. 2005. Preparation and sedimentation behavior in magnetic fields of magnetite-covered clay particles. *Langmuir* **21**, 4410-4419. (doi: 10.1021/la047393q)
16. Viota JL, Arroyo FJ, Delgado AV, Horno J. 2010. Electrokinetic characterization of magnetite nanoparticles functionalized with amino acids. *J Colloid Interface Sci* **344**, 144–149 (doi:10.1016/j.jcis.2009.11.061)
17. Illés E, Tombácz E. 2006. The effect of humic acid adsorption on pH-dependent surface charging and aggregation of magnetite nanoparticles. *J Colloid Interface Sci* **295**, 115–123. (doi:10.1016/j.jcis.2005.08.003)
18. Duran JDG, Ramos-Tejada MM, Arroyo FJ, Gonzalez-Caballero F. 2000. Rheological and electrokinetic properties of sodium montmorillonite suspensions. *J Colloid Interface Sci* **229**, 107–117 (doi:10.1006/jcis.2000.6956)
19. Abrougui MM, Belén Bonhome-Espinosa AB, Bahri D, López-López MT, Durán JDG, Srasra E. 2018. Rheological properties of clay suspensions treated by hydrocyclone process. *J Nanofluids* **7**, 258–268 (doi: https://doi.org/10.1166/jon.2018.1460)
20. Kara M, Yuzera H, Sabah E, Celik MS. 2003. Adsorption of cobalt from aqueous solutions onto sepiolite. *Water Res* **37**, 224–232. (doi: 10.1016/S0043-1354(02)00265-8)
21. Alkan M, Demirbas O, Mehmet Dogan M. 2005. Electrokinetic properties of sepiolite suspensions in different electrolyte media. *J Colloid Interface Sci* **281**, 240–248 (doi:10.1016/j.jcis.2004.08.036)
22. Xu J, Wang A. 2012. Electrokinetic and colloidal properties of homogenized and unhomogenized palygorskite in the presence of electrolytes. *J Chem Eng Data* **57**, 1586−1593. (dx.doi.org/10.1021/je300213u)
23. Zhang Z, Wang W, Wang A. 2015. High-pressure homogenization associated hydrothermal process of palygorskite for enhanced adsorption of Methylene blue. *Appl Surf Sci* **329**, 306–314. (http://dx.doi.org/10.1016/j.apsusc.2014.12.187)
24. Ahribesh AA, Lazarević S, Janković-Castvan I, Jokić B, Spasojević V, Radetić T, Janaćković D, Petrović R. 2017. Influence of the synthesis parameters on the properties of the sepiolite-based magnetic adsorbents. *Powder Technol* **305**, 260–269 (http://dx.doi.org/10.1016/j.powtec.2016.09.086)
25. Ramos-Tejada MM, de Vicente J, Ontiveros A, Duran JDG. 2001. Effect of humic acid adsorption on the rheological properties of sodium montmorillonite suspensions. *J Rheol* **45**, 1159-1172 (https://doi.org/10.1122/1.1392297)
26. Ramos-Tejada MM, Ontiveros A, Viota JL, Durán JDG. 2003. Interfacial and rheological properties of humic acid/hematite suspensions. *J Colloid Interface Sci* **268**, 85–95. (doi:10.1016/S0021-9797(03)00665-9)
27. Jiles DC. Introduction to magnetism and magnetic materials. Chapman & Hall, London; 1991. p. 115, p. 94. (doi: 10.1088/0022-3727/27/1/001)
28. Rosenweig RE. Ferrohydrodynamics. Cambridge University Press, New York; 1985, p. 58. (https://doi.org/10.1002/zamm.19870670626)
29. Kemp SJ, Ferguson RM, Khandhar AP, Krishnan KM. 2016. Kemp SJ, Ferguson RM, Khandhar AP, Krishnan KM. 2016. *Rsc Advanced* **6**, 77452-77464 Rsc Advanced 6, 77452-77464 (doi: 10.1039/c6ra12072e)
30. Norman J, Wagner NJ, Brady J. 2009. Shear thickening in colloidal dispersions. *Phys Today* **62**, 27-32 (doi: 10.1063/1.3248476 View online: https://doi.org/10.1063/1.3248476)
31. Kuzhir P, López-López MT, Bossis G. 2009. Magnetorheology of fiber suspensions. II. Theory. *J Rheol* **53**, 127–151. (https://doi.org/10.1122/1.3005405)
32. Gomez-Ramirez A, Kuzhir P, Lopez-Lopez MT, Bossis G, Meunier A, Duran JDG. 2010. Steady shear flow of magnetic fiber suspensions: Theory and comparison with experiments. *J Rheol* **55**, 43-67. (https://doi.org/10.1122/1.3523477)
33. Ana Gomez-Ramirez A, Lopez-Lopez MT, Duran JDG, Fernando Gonzalez-Caballero F. 2009. Influence of particle shape on the magnetic and magnetorheological properties of nanoparticle suspensions. *Soft Matter* **5**, 3888–3895. (doi: 10.1039/b906505a)
34. Bell C, Karli JO, Vavreck AN, Zimmerman DT, Ngatu GT, Wereley NM. 2008. Magnetorheology of submicron diameter iron microwires dispersed in silicone oil. *Smart Mater Struct* **17**, 015028 (6pp). (doi: 10.1088/0964-1726/17/01/015028)
35. Borin D, Odenbach S, Iskakova L, Zubarev A. 2018. Non-ergodic tube structures in magnetic gels and suspensions. *Soft Matter,* published online 18 October 2018. (doi: 10.1039/c8sm01456f)